High resolution reconstruction for 3D SPECT

Tianfang Li[*a], Junhai Wen[b], Hongbing Lu[b], Xiang Li[b], and Zhengrong Liang[b]
[a]Department of Physics and Astronomy, SUNY at Stony Brook, NY 11794, USA
[b]Department of Radiology, SUNY at Stony Brook, NY 11794, USA

ABSTRACT

In this work, we have developed a new method for SPECT (single photon emission computed tomography) image reconstruction, which has shown the potential to provide higher resolution results than any other conventional methods using the same projection data. Unlike the conventional FBP- (filtered backprojection) and EM- (expectation maximization) type algorithms, we utilize as much system response information as we can during the reconstruction process. This information can be pre-measured during the calibration process and stored in the computer. By selecting different sampling schemes for the point response measurement, different system kernel matrices are obtained. Reconstruction utilizing these kernels generates a set of reconstructed images of the same source. Based on these reconstructed images and their corresponding sampling schemes, we are able to achieve a high resolution final image that best represents the object. Because a uniform attenuation, resolution variation and some other effects are included during the formation of the system kernel matrices, the reconstruction from the acquired projection data also compensates for all these effects correctly.

Keywords: high resolution reconstruction, circular harmonic decomposition, conjugate gradient, fan-beam, uniform attenuation, resolution variation

1. INTRODUCTION

SPECT imaging has been quite useful in many diagnoses for its functional capability. However, it still suffers from relatively poor image quality as compared to other imaging modalities due to several degradation factors. First of all, because of the stochastic nature of photon emission from the radioactive source, noise always exists in the measured photon counts, which propagates in the reconstruction process and leads to fluctuation in the reconstructed images and poor visibility of the internal structures. Usually a low-pass filter with different cutoff frequencies is applied to suppress the noise in SPECT, but at the cost of image blurring in some degree. Secondly, the emitted gamma rays from an internal source may experience photoelectric absorption within the body or may be scattered away with no contributing to the acquired data. The degree of attenuation is determined by the linear attenuation coefficient, which depends on the photon energy and the amount and type of the materials contained in the attenuating medium. Attenuation is the most important factor that affects the quantitative accuracy of SPECT images. Thirdly, the scattered photons change their original flight path and energy with a false contribution to the data, causing lower image contrast and inaccurate quantitation in SPECT images. Fourthly, the survived photons from the body will be selectively detected by the collimated detection system, whose response can be characterized by a point spread function (PSF), also known as the system response function. For a typical collimated detector system, the PSF broadens as the distance from the source to the collimator surface increases, resulting in variable resolution blurring in the reconstructed image.

Great efforts have been devoted to the work for improving the SPECT imaging system, including different scintillation detectors and collimation designs [1-8]. Along with the hardware improvement, many research interests have also been focusing on compensations of all the degradation factors during the reconstruction processes [9-15]. In this work, we developed a new method for SPECT image reconstruction, which showed the potential to achieve very high spatial resolution. Unlike the conventional FBP- and EM-type algorithms, we utilize as much system information as we can during the reconstruction process. With the system information, we were able to gain a significant improvement on the reconstruction resolution, in addition to compensation for all degradation factors. Furthermore, our proposed method is computationally efficient, as compared to the EM-type reconstruction, and is applicable to parallel-hole, fan-beam, and varying focal-length fan-beam collimator geometries.

[*] tfli@clio.rad.sunysb.edu; phone 1 631 444-7999; fax 1 631 444-6450

Medical Imaging 2003: Image Processing, Milan Sonka, J. Michael Fitzpatrick, Editors,
Proceedings of SPIE Vol. 5032 (2003) © 2003 SPIE · 1605-7422/03/$15.00

2. METHODS

2.1 Detector intrinsic resolution, system resolution and detection power

For PET (positron emission tomography) imaging system, which does not need mechanic collimation, the detector intrinsic resolution and system resolution have the same meaning which is usually measured according to the NEMA test standards, and defined as the FWHM (full-width-at-half-maximum) of the reconstructed point/line source. For SPECT imaging system, the system resolution consists of detector intrinsic resolution and collimator geometric resolution and can be expressed as the detector intrinsic resolution in quadrature with the collimator geometric resolution [2]. It is determined not only by the design of the detector system but also by the reconstruction algorithms. For example, the system resolution of a typical parallel-hole collimated SPECT scanner is around 10 mm, and a dedicated system with fan-beam collimators and appropriate reconstruction algorithm for brain studies can improve the resolution to 5 mm [1].

Detection power of a SPECT system, however, is independent of the reconstruction algorithms, which we defined as the minimum distance between two locations of a point source that can be differentiated by the detector system. As illustrated in Fig. 1(a), when the point source is moved from A to B, there is a detectable change of the detector response from h_A to h_B. The detection power in nature gives the best resolution that we may achieve. Figure 1(b) shows difference between the system resolution measured from a reconstructed point source and the detector point response at each individual view position. In Fig. 1(c), we presented two different samplings that may be used to generate two different system kernel matrices, one is shifted from the other by a certain distance such that the detector system is able to perceive any change.

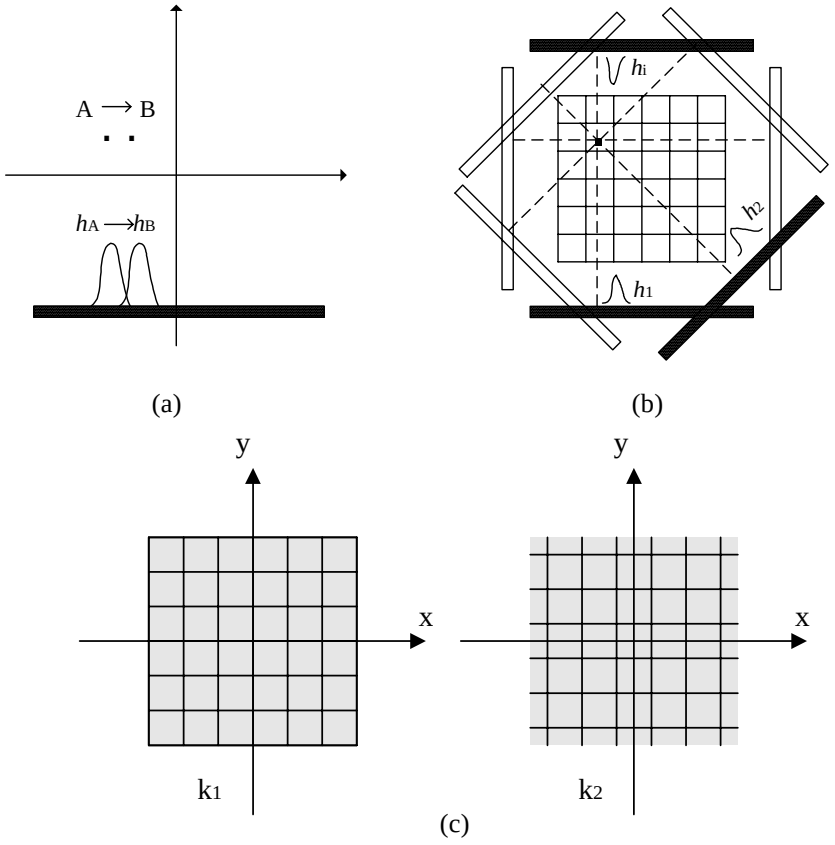

Figure 1. (a) Detection power -- the minimum distance between two locations of a point source that the detector can perceive the difference. (b) System resolution -- the FWHM of reconstructed point image. (c) Different sampling can generate different kernel matrices k_1 and k_2 – which can have different effect on the system resolution.

2.2 Circular symmetry in uniform attenuation

The system kernel matrix for general cases could be tremendously large. However, if symmetry is taken into account, the size can be reduced greatly. In Fig. 2, it is shown how a circular sampling can be used to construct the system kernel matrix in a fully 3D SPECT with inclusion of uniform attenuation.

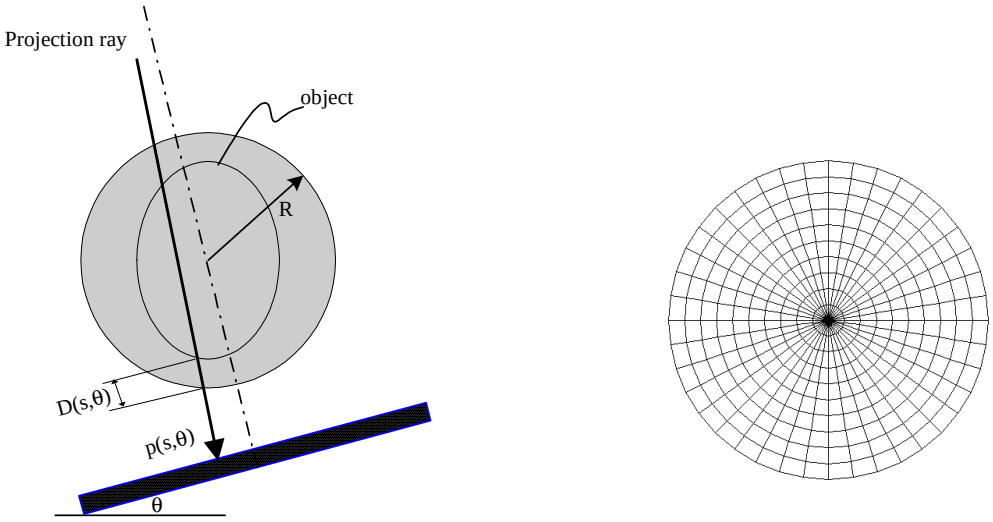

(a) (b)

Figure 2. (a) Modification for circular symmetry on uniformly attenuated projections. (b) Circular sampling for the system kernel matrix.

Although a general object usually does not have a circular symmetry, its projection data may be modified so that its attenuation map is equivalent to a uniform disk with radius R as shown in Fig. 2(a), if the object has a constant attenuation coefficient inside a convex boundary. It is easy to see that the modified projection p^m and the original projection p has the following relation

$$p^m(s,\theta) = e^{-uD(s,\theta)}\, p(s,\theta) \tag{1}$$

where $D(s,\theta)$ is the distance from the object boundary to the enlarged circle along the photon path. Thereafter the system imaging matrix k can be measured as the responses of each element inside the uniform-attenuation disk as shown in Fig. 2(b), and the modified projection can be expressed in polar coordinate system as

$$p^m(s,\theta) = \sum_{\rho,\varphi} f(\rho,\varphi) k(\rho,\theta-\varphi,s)\Delta_{\rho,\varphi} \tag{2}$$

where $\Delta_{\rho,\varphi}$ is the area of the finite element at location (ρ,φ), $f(\rho,\varphi)$ is the average activity at the same location, and matrix k consists of the responses of all elements Δ.

In three dimensions, the object can be modified to be a uniform-attenuation cylinder by the same strategy, and equations (1) and (2) become

$$p^m(s,\theta,z) = e^{-uD(s,\theta,z)}\, p(s,\theta,z) \tag{3}$$

$$p^m(s,\theta,z) = \sum_{\rho,\varphi,z'} f(\rho,\varphi,z') k(\rho,\theta-\varphi,z-z',s)\Delta_{\rho,\varphi,z'} \tag{4}$$

2.3 Method to improve the resolution

It has been shown that equation (2) or (4) can be used to solve for the object activity distribution f. For example, after a two-dimensional (2D) Fourier transform (FT) on θ and z of equation (4), we get

$$P_{n,\omega}^{m}(s) = \sum_{\rho} F_{n,\omega}(\rho) K_{n,\omega}(\rho, s) \tag{5}$$

where

$$P_{n,\omega}^{m}(s) = \int_{0}^{2\pi} d\theta \int_{-\infty}^{\infty} dz \; p^{m}(s,\theta,z) e^{-i(n\theta+\omega z)} \tag{6}$$

$$F_{n,\omega}(\rho) = \int_{0}^{2\pi} d\varphi \int_{-\infty}^{\infty} dz \; f(\rho,\varphi,z') e^{-i(n\varphi+\omega z')} \tag{7}$$

$$K_{n,\omega}(\rho, s) = \int_{0}^{2\pi} d\theta \int_{-\infty}^{\infty} dz \; \rho k(\rho,\theta,z,s) e^{-i(n\theta+\omega z)} \tag{8}$$

Equation (5) is equivalent to $P=KF$, (the subscripts n and ω are omitted for simplicity), where K is a complex matrix and can be written as $K=K_1+iK_2$, F and P are the complex image vector and projection vector in terms of harmonic coefficients, $F=F_1+iF_2$, and $P=P_1+iP_2$. Define

$$Q = \begin{pmatrix} K_1^T K_1 + K_2^T K_2 & -K_1^T K_2 + K_2^T K_1 \\ -K_2^T K_1 + K_1^T K_2 & K_1^T K_1 + K_2^T K_2 \end{pmatrix}, \; b = \begin{pmatrix} K_1^T P_1 + K_2^T P_2 \\ -K_2^T P_1 + K_1^T P_2 \end{pmatrix} \tag{9}$$

where the superscript T denotes the transpose of a matrix or a vector. Let $F^k=F_1^k+iF_2^k$ be the k-step estimate of F, using the conjugate gradient algorithm, we have the following iterative procedure for the solution:

$$x^{k+1} = x^k + \alpha_k d_k \qquad \alpha_k = -\frac{g_k^T d_k}{d_k^T Q d_k} \tag{10}$$

$$d_{k+1} = -g_k + \beta_k d_k \qquad \beta_k = \frac{g_{k+1}^T Q d_k}{d_k^T Q d_k}$$

where $x^k = \begin{pmatrix} F_1^k \\ F_2^k \end{pmatrix}$, $d_0=-g_0$, and $g_k=Qx^k-b$. After $F_{n,\omega}$ is achieved, the source activity distribution f is then uniquely determined. This reconstruction method is also referred as the circular harmonic decomposition - conjugate gradient algorithm (CHD-CG) [16, 17].

To improve the resolution, we note that the reconstruction result is completely determined by the system kernel matrix, given the acquired data. The kernel matrix is the response of each sampling point that we have chosen. It is expected that different sampling schemes shall result in different system responses, hence produce different kernel matrices. Figure 3(a) shows some examples of sampling schemes as illustrated in transverse plane and axial plane. On the other hand, a reconstructed image represents the estimated activity distribution of the source on the sampled points defined by a sampling scheme. It is assumed that reconstruction using different matrices shall result in different images about the same source, which only differ due to the different sampling means. Based on these reconstructed images and their corresponding sampling schemes, it is our goal to obtain a final image with highest resolution that best presents the source.

For example, let f_1 and f_2 be the reconstructed images using two different kernel matrices shown in Fig. 3(a) transverse plane, and f be the unknown activity distribution at a finer grid shown in Fig. 3(b) transverse plane. Note that there are relations among the samplings as shown in Fig. 3(c):

$$f_1^i = w_{2i} f^{2i} + w_{2i+1} f^{2i+1} \tag{11}$$

$$f_2^i = w_{2i-1} f^{2i-1} + w_{2i} f^{2i} \tag{12}$$

In equation (11), f_1^i is the intensity at pixel i in a common reconstruction image f_1, which is the weighted summation of the intensities of two subdivided pixels f^{2i} and f^{2i+1} in a higher resolution image, w_i is the weight. Equation (12) has the similar meaning. Therefore, estimation of f with nearest five neighbors using equations (11) and (12) is given by

$$f^{2i} = \frac{1}{2}(f_1^i + f_2^i) - \frac{1}{3}(f_1^{i-1} + f_2^{i+1}) + \frac{1}{3}(f_1^{i+1} + f_2^{i-1}) - \frac{1}{12}(f_1^{i-2} + f_2^{i+2}) + \frac{1}{12}(f_1^{i+2} + f_2^{i-2}) \qquad (13)$$

$$f^{2i+1} = \frac{1}{2}(f_1^i + f_2^{i+1}) - \frac{1}{3}(f_1^{i+1} + f_2^i) + \frac{1}{3}(f_1^{i-1} + f_2^{i+2}) - \frac{1}{12}(f_1^{i+2} + f_2^{i-1}) + \frac{1}{12}(f_1^{i-2} + f_2^{i+3}) \qquad (14)$$

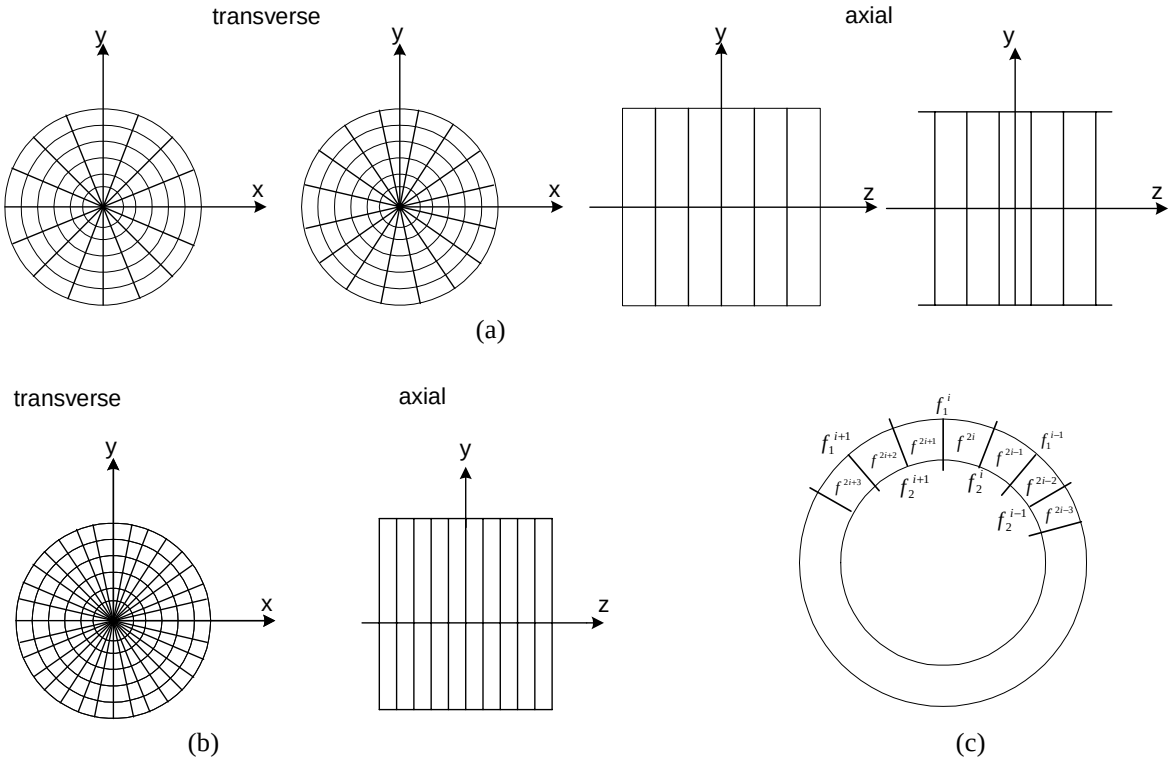

Figure 3. (a) Sampling schemes in transverse plane and axial plane for generating the system kernel matrices. (b) Sampling at finer grids. (c) Relation between samplings in transverse plane, e.g., $f_1^i = w_{2i} * f^{2i} + w_{2i+1} * f^{2i+1}$, and $f_2^i = w_{2i-1} * f^{2i-1} + w_{2i} * f^{2i}$.

The implementation for the proposed high-resolution reconstruction includes the following steps:

(1) Measure kernel matrices according to different sampling schemes during the calibration stage with inclusion of uniform attenuation. To get a kernel matrix, a point source is moved at different radial positions and the corresponding system responses are measured at all view angles for each source location. The measured kernel matrices are then normalized and stored in computer;

(2) Scan for the projection data in application;

(3) Reconstruct the images with different kernel matrices using the described CHD-CG algorithm;

(4) Estimate the final image using equation (13) and (14) with the reconstructed images obtained from step (3).

3 EXPERIMENT RESULTS

The proposed method was tested with simulated SPECT projection data of 64x64 size using two different digital phantoms and uniform attenuation map in a fan-beam (FB) collimator geometry. The experimental setup was as

follows: the modeled low-energy high-resolution FB collimator was 44 cm wide, 2.7 cm thick, hexagonal holes with side of 0.14 cm on front surface. The focal length of the collimators was 82.5 cm. The crystal was NaI(Tl) with thickness of 1.588 cm. The data simulation experiment is similar to a clinical setting (except for Poisson noise and Compton scatter).

In the calibration stage, the kernel matrices corresponding to the sampling schemes of Fig. 3(a) transverse plane were measured with a ^{99m}Tc point source, and the total counts were set as high as 10 million in order to suppress the effect of noise. The measured kernel matrices were then normalized to 1 and stored in computer. Then sinograms of size 128x64 pixels were simulated using different phantoms. The total counts were set to 20 million for all 64 views.

In reconstruction, the CHD-CG algorithm of equation (10) was applied to generate several intermediate reconstructed images with resolution of 128x64, and finally a 128x128 resolution image was obtained. The reconstruction was calculated in polar coordinate system, and the images were then mapped to Cartesian coordinate system using linear interpolation for illustration purpose. The first experiment was to reconstruct the Shepp-Logan phantom, and the second one was for the Hoffman phantom. From the results, we observed that more details have been restored from the low resolution reconstruction images, see Figures 4 and 5.

(a) (b) (c) (d)

Figure 4. Experimental study with the Shepp-Logan phantom -- (a) is the original phantoms; (b) and (c) are two intermediate reconstruction images with normal resolution; and (d) is the final image using our proposed method with doubled resolution.

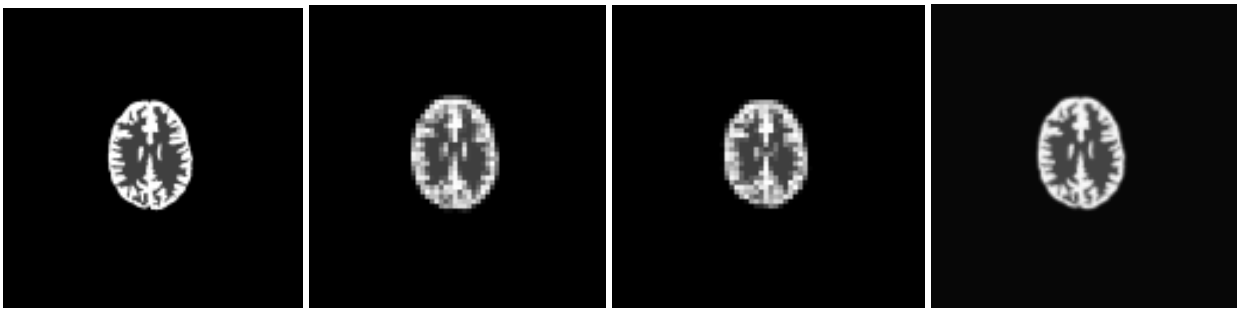

(a) (b) (c) (d)

Figure 5. Experimental study with the Hoffman phantom -- (a) is the original phantoms; (b) and (c) are two intermediate reconstruction images with normal resolution; and (d) is the final image using our proposed method with doubled resolution.

4 CONCLUSIONS

The experiments show that it is possible to obtain higher resolution reconstruction image for SPECT using our proposed methods than conventional FBP methods. The achieved improvement is because more system information is adopted into the reconstruction process. With one scanned data, the source activity distribution at more sampled locations were estimated, therefore a more accurate estimation of the source object can be achieved. Furthermore, the computation of this method is relatively efficient. This computational advantage is mainly because that the system kernel matrix is greatly reduced with symmetry incorporated. Its advantage over the EM-type iterative algorithms is more clearly seen

because of the following reasons. First, this method is using one matrix which considered all factors together rather than tracing the projection process sequentially using several models. Secondly, the method decomposes the 3D problem into 1D linear equations. For each slice and each view the linear equations are independent and can be computed simultaneously. This parallel ability could further save a significant computation time.

However, this method has its own disadvantage as any other iterative algorithm does. The solution to the problem is not exact but only an estimation of the real source. Due to the reason that the system matrix is usually not invertible, the solution to the linear equations is often an estimation using iterations. Therefore, the final image, generated based on the estimations, is not the exact solution but a better estimation.

ACKNOWLEGEMENTS

This work was supported in part by a NIH grant #HL51466 and a SNM student fellowship award (Summer of 2002).

REFERENCES

1. T. Ichihara, K. Nambu. N. Motomura, "High spatial resolution reconstruction technique for SPECT using a fan-beam collimator", *IEEE Trans. Nucl. Sci.*, **40:** 1149-1153, 1993.
2. S. J. Glick, "The effect of intrinsic spatial resolution on the quantitative accuracy of SPECT imaging", *IEEE Trans. Nucl. Sci.*, **46**:1009-1015, 1999**.**
3. R. J. Jaszczak, L. T. Chang, P. H. Murphy, "Single photon emission computed tomography using multi-slice fan beam collimators", *IEEE Trans. Nucl. Sci.*, **26:** 610-618, 1979.
4. C. B. Lim, L. T. Chang, R. J. Jaszczak, "Performance analysis of three camera configuration for single photon emission computed tomography", *IEEE Trans. Nucl. Sci.*, **27:** 559-568, 1980.
5. B. M. W. Tsui, G. T. Gullberg, E. R. Edgerton, D. R. Gilland, J. R. Perry, and W. H. McCartney, "Design and clinical utility of a fan beam collimator for SPECT imaging of the head", *J. Nucl. Med*., **27:** 810-819, 1986.
6. J. Hsieh, *Scintillation camera and multifocal fan-beam collimator used therein*, United States Patent 4,823,017, 1989.
7. R. J. Jaszczak, J. Li, H. Wang, and R. E. Coleman, "SPECT collimation having spatially variant focusing (SVF)", *J. Nucl. Med*., **33:** 891, 1992.
8. B. M. W. Tsui, X. D. Zhao, P. Vemon, D. Nowak, J. R. Perry, and W. H. McCartney, "Cardiac SPECT reconstructions with truncated projections in different SPECT system designs", *J. Nucl. Med*., **33:** 831, 1992.
9. J. Cheng, Z. Liang, J. Ye, C. Cabahug, Z. Oster, and D. Harrington, "Accurate treatment of possion noise for quantitative reconstruction of brain SPECT", *J. Nucl. Med*., **37:** 218, 1996.
10. H. Lu, G. Han, D. Chen, L. Li, and Z. Liang, "A theoretically based approach to noise reduction in SPECT by Anscombe and KL transforms", *J. Nucl. Med*., **41:** 198, 2000.
11. X. Li, G. Han, H. Lu, L. Li, and Z. Liang, "A new scatter estimation method using triple window acquisition to fit energy spectrum", *J. Nucl. Med*., **42:** 194, 2001.
12. G. L. Zeng and G. T. Gullberg, "A backprojection filtering algorithm for a spatially varying focal length collimator", *IEEE Trans. Med. Imag*., 13: 549-556, 1994.
13. X. Pan, C. E. Metz, and C.-T. Chen, "A class of analytical methods that compensate for attenuation and spatially-variant resolution in 2D SPECT", *IEEE Trans. Nucl. Sci*., **43:** 2244-2254, 1996.
14. S. J. Glick, B. C. Penney, M. A. King, and C. L. Byrne, "Noniterative compensation for the distance-dependent detector response and photon attenuation in SPECT imaging", *IEEE Trans. Med. Imag*., **13:** 363-374, 1994.
15. G. Han, Z. Liang, "A fast projector and back-projector for SPECT with varying focal-length fan-beam collimators", *J. Nucl. Med*., **40:** 301, 2000.
16. J. You and Z. Liang, "A harmonic decompostion approach to compensate for uniform attenuation and collimator response in fan-beam collimated brain SPECT", *Intl. Conf. Fully 3D Image Reconstruction in Radiology and Nuclear Medicine*, Holland, 243-246, 1999.
17. J. You, Z. Liang and S. Bao, "A harmonic decomposition algorithm for spatially varying focal length fan-beam collimators", *IEEE Trans. Med. Imag.*, **17:** 955-1002, 1998.